

Initial Results from the Infrared Calibration and Infrared Imaging of a Microwave Calibration Target *

Amanda E. Cox¹, Joseph J. O'Connell², and Joseph P. Rice²

¹Electromagnetics Division, ²Optical Technology Division
National Institute of Standards and Technology
Boulder, CO 80305, U.S.A.

Abstract—As part of the ongoing effort at NIST to develop a microwave brightness temperature standard, we are exploring the electromagnetic and thermal characteristics of microwave calibration targets. We investigate the thermal properties of a microwave calibration target using NIST infrared calibration facilities and techniques. An infrared radiometer is used to measure the radiance at the surface of a microwave calibration target and to compare it with the values reported from contact temperature sensors. We find temperature gradients within the target greater than 1 K. Infrared imagery shows temperature gradients within the geometric structure of the target.

Keywords—brightness temperature; infrared calibration; microwave calibration; microwave radiometry; radiometer calibration; remote sensing

I. INTRODUCTION

Microwave radiometers are calibrated by having them view sources of known brightness temperature. For remote sensing radiometers, calibration is commonly achieved by viewing one or more calibration targets in free space through the radiometer feed or antenna. These calibration targets are designed to approximate blackbody sources over the frequencies of interest. The microwave brightness temperature available to the radiometer from the calibration source is a function of the physical temperature of the target and its emissivity. The physical temperature of the target is typically measured using temperature sensors embedded in the target substrate, and a weighted average of the sensors, along with the emissivity value, is used to calculate the effective brightness temperature during the calibration of sensor data. In some targets, temperature gradients can exist both across the target face, and between the heated substrate and the surface viewed by the radiometer. These gradients can give rise to large uncertainties with respect to the brightness temperature received at the radiometer aperture, thus affecting its calibration and the accuracy of the data products derived from the instrument. A few studies have been conducted to observe and/or quantify these thermal gradients [1], [2], [3]; we expand upon these efforts to develop a method to better characterize calibration target properties.

NIST maintains and disseminates the national measurement scales for radiance measurements in the ultraviolet, visible, and infrared spectral regions [4]. NIST also maintains primary

noise standards in the microwave spectral region and is developing a microwave brightness temperature standard that links back to those primary standards. The proposed microwave brightness temperature standard [5] includes a standard target consisting of a well-characterized calibration target that would produce a known brightness temperature. In order to have a well-characterized calibration target, we need to understand its thermal performance. As a part of this effort, we studied the performance of a microwave calibration target in the infrared portion of the spectrum. The techniques we developed have the potential benefit of providing much insight into the performance of microwave calibration targets. These methods can provide detailed information on the relationship between the observed target surface and the temperature monitoring devices; the measurements can quantify the temperature gradients existing within the target, and they can provide a detailed image of the overall target thermal characteristics.

Using a typical microwave calibration target and the infrared calibration facilities in our Gaithersburg, MD location, we calibrated portions of the microwave target with respect to the embedded platinum resistance thermistors (PRTs) and imaged the target using two different thermal-imaging arrays. To measure the infrared brightness temperature, we viewed the target with the NIST Thermal-infrared Transfer Radiometer (TXR) [6]. The TXR radiometer was developed for use in intercomparisons and scale verifications of sources used to calibrate thermal-infrared (TIR) channels. It was designed to measure the radiance temperature of large-area blackbody sources in cryogenic vacuum environments, but can also be operated in ambient conditions of room temperature and pressure. The field of view of the TXR was limited to a few pyramids of the target structure, and the measurements provide information on the gradient between the embedded temperature sensor and the target surface as well as linking the calibration target's thermal properties back to a NIST standard. The imaging arrays provide information on the thermal gradients that occur across the face of the target. Both of these imagers viewed the target with a spatial resolution sufficient to resolve intra-pyramid brightness temperature gradients with several pyramids in the full field of view.

In Section II we outline the measurement methods used for both the TXR and imagers. Section III presents the approach

* U.S. Government work; not protected by U.S. copyright.

and initial results for this experiment. Section IV contains a summary and discussion of future work.

II. MEASUREMENT SYSTEM

The TXR and infrared imagers were mounted on a platform of an automated 3-axis precision positioning system. This structure was then mounted on an optical bench in the NIST IR calibration facility. The microwave calibration target was mounted opposite the platform on a separate 2-axis positioning system. The experiment was conducted at ambient temperature and pressure in a shielded chamber that reduced convection currents around the instruments and kept out stray radiation. The environment was not stringently controlled, but the shielding created a relatively stable thermal environment. A laser was used to align the TXR aperture on specific pyramids of the microwave target. Figure 1 is a photograph of the experiment. The microwave calibration target is on the left, while the TXR dewar can be seen behind the imaging cameras on the right. The black plate in front of the dewar is the TXR scene plate. Details of the equipment are described below.

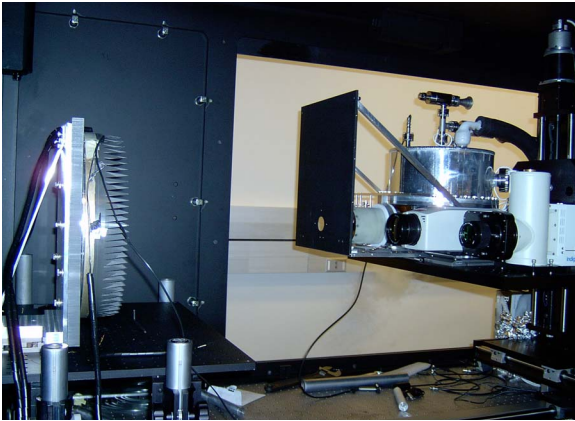


Figure 1. Photograph of the experimental set-up

A. Thermal-infrared Transfer Radiometer (TXR)

The TXR is a liquid-nitrogen cooled filter radiometer with two channels. Channel 2 has a center wavelength of 10 μm with a 1 μm wide bandpass. Channel 1 has a center wavelength of 5 μm , but is not used in this test because the signal is affected excessively by water vapor absorption in the ambient environment. The absolute calibration of the TXR radiance scale is traceable via an on-board infrared blackbody to a NIST high-accuracy infrared cavity radiometer, the Water Bath Blackbody (WBBB) [7]. Data collected using the WBBB were transferred to the on-board blackbody or check source (CS), and the CS was then used to maintain the TXR calibration scale for these measurements. The TXR has a field of view of 30 milliradians and was positioned to view approximately one pyramid of the microwave target structure at a time.

B. Infrared Cameras

Two different infrared imaging cameras were used to observe the heated microwave target. Both cameras read array values out to a computer file and allow image capture. One of

the imagers uses a liquid nitrogen cooled 320 x 256 InSb array, and has a spectral bandpass from 2 μm to about 5.5 μm . The other imager uses an uncooled 320 x 240 microbolometer array, and has a spectral bandpass from 7 μm to 13 μm . The cameras were mounted side by side on the positioner platform next to the TXR. The camera-target distance was adjusted as necessary to fit a significant portion of the target into the field of view while maintaining focus.

C. Microwave Calibration Target

The microwave target used for these measurements was borrowed from NASA Goddard Space Flight Center (GSFC). The target is a commercially produced circular disc approximately 33 cm in diameter. The surface is covered with an array of square-based pyramids with an aspect ratio of 4:1. The base material of the target is aluminum, with pyramids formed by electrical discharge machining (EDM) and coated with ferrous-loaded epoxy to a thickness of about 1 mm. The physical temperature of the calibration target was monitored by five PRTs embedded in back of the target base. An additional PRT was used to monitor the ambient environment. A custom heating element, adhered to the target base, was used in conjunction with a closed-loop control system to heat the target from 300 to 340 K in 5 K increments allowing time for temperature stabilization between each change. In some cases, the target was allowed to equilibrate thermally overnight.

III. MEASUREMENTS

A. Approach

The TXR data were analyzed by the following model. The response [in millivolts], $r_2(T)$, of TXR Channel 2 (hence the subscript 2) to any blackbody (BB) is given by the measurement equation,

$$r_2(T) = \int R_{2\lambda}(\lambda) \cdot \varepsilon(\lambda) \cdot B(\lambda, T) d\lambda + \int R_{2\lambda}(\lambda) \cdot [1 - \varepsilon(\lambda)] \cdot B(\lambda, T_o) d\lambda, \quad (1)$$

where T is the thermodynamic temperature [K], λ is the wavelength [μm], ε is the BB emissivity, $R_{2\lambda}(\lambda)$ is the absolute spectral responsivity of TXR Channel 2, and $B(\lambda, T)$ is the spectral radiance [$\text{W}/(\text{cm}^2 \cdot \text{sr} \cdot \text{nm})$] from the Planck function,

$$B(\lambda, T) \equiv \frac{c_{1L}}{\lambda^5 [\exp(c_2 / (\lambda T)) - 1]}. \quad (2)$$

The function $R_{2\lambda}(\lambda)$ can be quantified in terms of an idealized box-car absolute responsivity function that has a constant magnitude of R_2 between two wavelengths, λ_{2lo} and λ_{2hi} , and is zero elsewhere. The fundamental radiation constants, c_{1L} and c_2 , and values for R_2 , λ_{2lo} , and λ_{2hi} are listed in Table 1. The TXR calibration of Channel 2 is then naturally quantified in terms of the band-integrated radiance from an ideal blackbody, $L_{B2}(T)$, defined as

$$L_{B2}(T) \equiv \int_{\lambda_{2lo}}^{\lambda_{2hi}} B(\lambda, T) d\lambda. \quad (3)$$

Calibrated band-integrated radiance values resulting from response measurements are defined as

$$L_{X2}(T_c) \equiv \frac{r_{X2}(T_c)}{R_2}, \quad (4)$$

where the subscript “X” denotes values from when the TXR viewed the microwave target, and T_c is the chosen PRT reading from the microwave target. Calibration of the TXR was performed against the WBBB from 17.5 °C to 85 °C to obtain R_2 . Since R_2 is independent of temperature, it was then used in Eq. (4) to convert r_{X2} to L_{X2} .

TABLE I. CALIBRATION PARAMETERS FOR THE TXR.

| Parameter Name | Symbol | Units | Channel 2 Value |
|--|-----------------|-------------------------|---------------------------|
| First radiation constant for spectral radiance | c_{1L} | W·m ² /sr | 1.19104×10^{-16} |
| Second radiation constant | c_2 | m·K | 1.43878×10^{-2} |
| TXR low wavelength band edge | λ_{2lo} | μm | 9.645 |
| TXR high wavelength band edge | λ_{2hi} | μm | 10.595 |
| TXR responsivity (from calibration with WBBB 4 cm) | R_2 | mV·m ² ·sr/W | 5.81472 |

Because L_{X2} itself varies strongly with T_c , the quantity analyzed for comparison of the microwave target to a blackbody is the difference between the measured radiance while observing the microwave target and the ideal blackbody radiance (by using T_c in Eq. 3),

$$\Delta L_2(T_c) \equiv L_{X2}(T_c) - L_{B2}(T_c). \quad (5)$$

In computing $\Delta L_2(T_c)$, a small out-of-field component is also subtracted from the TXR data, during both WBBB calibration and use, based upon the TXR’s out-of-field response to its scene plate.

B. Results

Results for two data sets are presented. For one component of the experiment, we compare the measurement for the peak of one pyramid to that for an adjacent valley. TXR data were taken while the TXR field of view was centered on one pyramid, repositioned to the valley, then back to the original peak. Figure 2 shows a plot of $\Delta L_2(T_c)$ vs. $L_{B2}(T_c)$ of Eq. (5) for one pyramid. The quantity $L_{B2}(T_c)$ was computed from the values of the nearest PRT for T_c . The TXR data were calibrated by adjusting its responsivity such that the average of the WBBB data at 4 cm is in agreement with that expected from an ideal blackbody (the straight line at zero in Figure 2). The actual WBBB data are shown in black x’s. Note that the two

sets of peak measurements (blue circles and green diamonds) closely track each other, while the valley has a bias with respect to these values. This bias corresponds to a temperature difference of approximately 0.03 K. A jump in the data coincides with a break in the data session where the target temperature was allowed to equilibrate overnight. This is due either to drift of the TXR or to changed gradients in the target after the long period of thermal equilibration.

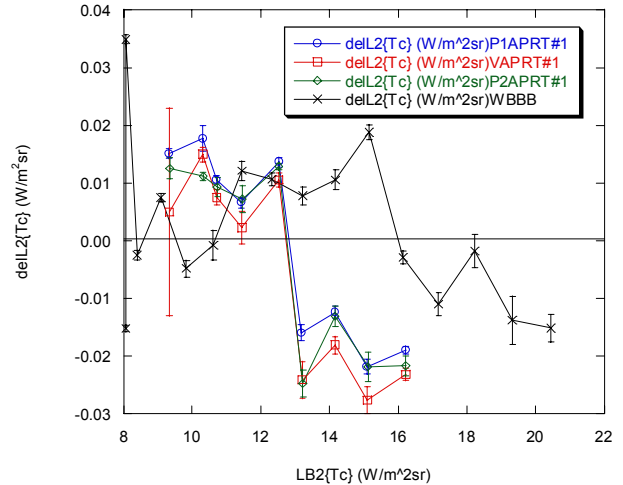


Figure 2. Radiance difference for PRT #1

The agreement of the microwave target radiance with the WBBB data (and hence the TXR scale) is within 0.1% at temperatures below the 325 K point, and appears to drop by no more than 0.2% at temperatures above that point. This is essentially within the TXR measurement uncertainty.

For another component of the experiment, we compare the results when different PRTs are used for the reference temperature. This was done for two pyramid locations, A and B. Figures 3 and 4 show the measured radiance at a pyramid location using different PRT readouts for T_c in computing $L_{B2}(T_c)$ from the Planck formula.

Figure 3 is a plot of $\Delta L_2(T_c)$ vs. $L_{B2}(T_c)$ at pyramid A using values from three of the PRTs. Two of the five target PRTs failed during the course of this experiment, one was damaged during shipping, and the other produced erratic results later attributable to the lead wires being pinched in the heater assembly. The data for PRT #1 are closest to the WBBB data since that PRT is located nearest the pyramid that the TXR viewed. As more distant PRTs are used, the error grows, and values decrease as temperature is increased. Note that on the scale of this plot, the break in the data coincident with the change of data sessions is barely perceptible.

Data from PRT #1 in Figure 3 are used to estimate the IR emissivity at 0.998 or better. When there is a negative slope to the $\Delta L_2(T_c)$ vs. $L_{B2}(T_c)$ plot, it usually indicates emissivity less than one, or strong temperature gradients between the PRT and the radiating surface. We see this trend for both PRT #2 and PRT #5. Typically this temperature trend shows up in the plot as a downward curve with increasing radiance so that the data are represented by a parabola rather than a straight line, but we

do not have as many temperature points as are taken with other blackbodies. Since the emissivity estimate from PRT #1 is nearly 1.0, this indicates that there are temperature gradients between the locations of PRTs 2 and 5 and pyramid A. These gradients are on the order of 1.25 K over distances of ~ 10 cm.

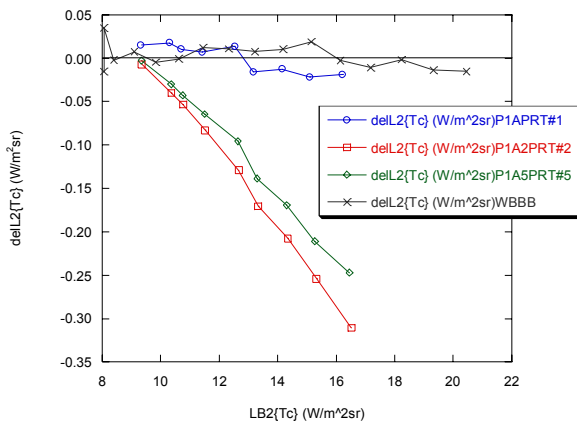


Figure 3. PRT dependence for pyramid A

Figure 4 shows $\Delta L_2(T_c)$ vs. $L_{B2}(T_c)$ for pyramid B. In Figure 4, we see the same trend for PRTs #2 and #5, as well as a slight downward slope for PRT #1. Pyramid B is farther away from PRT #1 than pyramid A, so we would expect to see a gradient for PRT #1 as well.

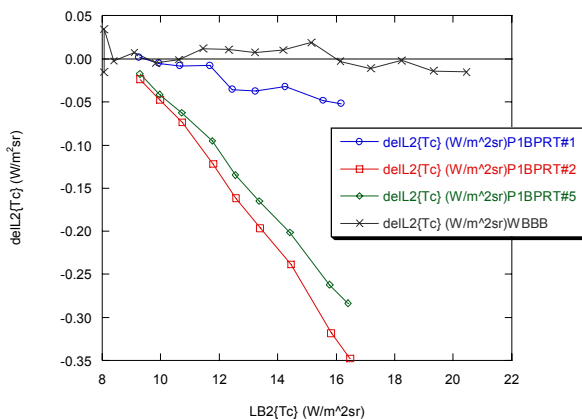


Figure 4. PRT dependence for pyramid B

Figure 5 shows an IR image of a portion of the microwave target. The geometric structure can be seen in this image; both the tips of the pyramids and the valleys between them are visible in this image. The lighter dots correspond to the lower temperature of the tips of the pyramids (recall that the target is heated at the base). The linear features of the valleys can be seen between the pyramids. The blue vertical line right of center and the blue horizontal region at the bottom of the image are artifacts of the imager and should be ignored. The image also shows that for this particular target and temperature, there is not a large gradient across the face of the target.

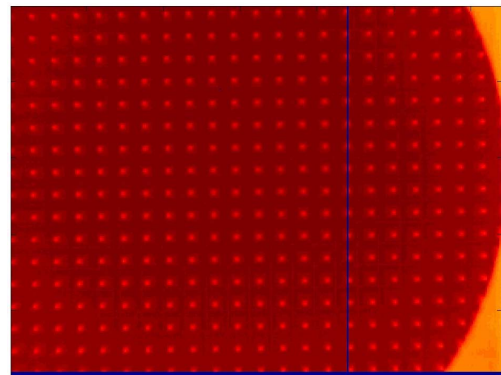


Figure 5. Infrared image of the microwave calibration target

IV. SUMMARY

We have presented the initial results from the infrared calibration of a microwave target. We have shown that we can quantify the temperature gradients in the target, including those between the PRT and the radiating surface and between one area on the target and another. The infrared imagery gives a display of these gradients over a larger physical scale than the TXR data. Both of these methods contribute to a greater understanding of the overall target performance and in the future can be used to fully characterize a calibration source.

Not all of the data from these experiments have been fully analyzed. Future work includes relating data from specific target positions to data from PRTs embedded at different depths within the target base and studying the z-direction dependence (if any) for the distance between the TXR and the target. Work is underway to achieve an absolute calibration of the imagery data from both infrared cameras.

ACKNOWLEDGMENT

The authors are grateful to P. Racette and J. Piepmeier of NASA Goddard Space Flight Center for the loan of the microwave calibration target and for helpful discussions.

REFERENCES

- [1] McGrath, A., T. Hewison, "Measuring the Accuracy of MARSS – An Airborne Microwave Radiometer," *Journal of Atmospheric and Oceanic Technology*, Vol. 18, no. 12, pp. 2003-2012. Dec 2001.
- [2] Cox, A.E., "Methods for Improving Microwave Radiometer Calibration and Data Quality for Geophysical Applications," 2003, Thesis, University of Colorado.
- [3] Jackson, D.M., "Calibration of Millimeter-Wave Radiometers with Application to Clear-Air Remote Sensing of the Atmosphere," 1999, Thesis, Georgia Institute of Technology.
- [4] <http://physics.nist.gov/Divisions/Div844/div844.html/>
- [5] J. Randa, A.E. Cox, and D.K. Walker, "Proposed Development of a National Standard for Microwave Brightness Temperature," 2006 IEEE International Geoscience and Remote Sensing Symposium Digest, to be published, Denver, CO, August 2006.
- [6] Johnson, B. Carol. Rice, J.P., "The NIST EOS Thermal-Infrared Transfer Radiometer," *Metrologia*, October 01, 1997.
- [7] Fowler, J. B., "A Third Generation Water Bath Based Blackbody Source," *J. Res. NIST* 100, 591, 1995.

**2006 International Geoscience and Remote Sensing Symposium Digest
(IGARSS-2006)
Denver, CO, U.S.A.
August, 2006**